MYSTERIOUS QUANTUM EFFECTS OBSERVED WITH NEUTRONS

H. RAUCH

Atominstitut, Vienna University of Technology
(1020 Wien, Austria; e-mail: xx@jjj)

PACS 98.62.Sb

Single-particle interference phenomena can be observed with neutrons, and the "entanglement of degrees of freedom", i.e. the contextuality, can be verified and used in further experiments. Entanglement of two photons or atoms is a complementary situation to the double-slit diffraction of a single photon, neutron, or atom. In this respect, neutrons are proper tools for testing quantum mechanics, because they are massive, they couple to electromagnetic fields due to their magnetic moment, and they are subject to all basic interactions, and they are sensitive to topological effects as well. The 4π-symmetry of spinor wave functions, the spin-superposition law, and many topological phenomena can be made visible, which shows interesting intrinsic features of quantum physics. Related experiments will be discussed. Deterministic and stochastic partial absorption experiments can be described by Bell-type inequalities. Recent neutron interferometry experiments based on post-selection methods have renewed the discussion about quantum non-locality and the quantum measuring process. It has been shown that interference phenomena can be revived even when the overall interference pattern has lost its contrast. This indicates a persisting coupling in the phase space even in cases of spatially separated Schrödinger cat-like situations. These states are extremely fragile and sensitive against any kind of fluctuations and other decoherence processes. More complete quantum experiments also show that a complete retrieval of quantum states behind an interaction volume becomes impossible in principle.

1. Introduction. Basic Relations

Neutrons have to be considered throughout this article as waves underlying the duality features of quantum physics. Experiments reported in this article have been performed with monochromatic low-energy neutrons from a research reactor and with neutron interferometers based on the wave-front and amplitude divisions [1–4]. The most frequently used neutron interferometer is a perfect crystal interferometer first tested in 1974 at our 250 kW TRIGA reactor. The wide beam separation of several centimeters and the relatively high intensity make it useful for fundamental-, nuclear-, and solid-state physics investigations [5] (Fig. 1).

The basis for this kind of neutron interferometry is provided by the undisturbed arrangement of atoms in a monolithic perfect silicon crystal [2, 6]. An incident beam is split coherently at the first crystal plate, reflected at the middle plate, and coherently superposed at the third plate. The general symmetry considerations imply immediately that the wave functions in both beam paths, which compose the beam in the forward direction behind the interferometer, are equal ($\psi_0^{\mathrm{I}} = \psi_0^{\mathrm{II}}$), because they are transmitted-reflected-reflected (TRR) and reflected- reflected-transmitted (RRT), respectively. The theoretical treatment of the diffraction process from the perfect crystal is described by the dynamical diffraction theory [7, 8]. To preserve the interference properties over the length of an interferometer, the lattice planes have to be parallel within one lattice constant, and the dimensions of the monolithic system have to be accurate on a scale comparable to the so-called Pendellösung length ($\sim 50\ \mu$m). The whole interferometer crystal has to be placed on a stable goniometer table under conditions avoiding temperature gradients and vibrations. A phase shift between the two coherent beams can be produced by nuclear, magnetic, or gravitational interactions. In the first case, the phase shift for non-absorbing and weakly absorbing materials is most easily calculated, by using the index of refraction [9, 10]:

$$n = \frac{k_{in}}{k_0} = 1 - \frac{\lambda^2 N}{2\pi}\sqrt{b_c^2 - \frac{\sigma_r^2}{2\lambda}} + i\frac{\sigma_r N\lambda}{4\pi} \cong 1 - \lambda^2\frac{Nb_c}{2\pi}\ , \tag{1}$$

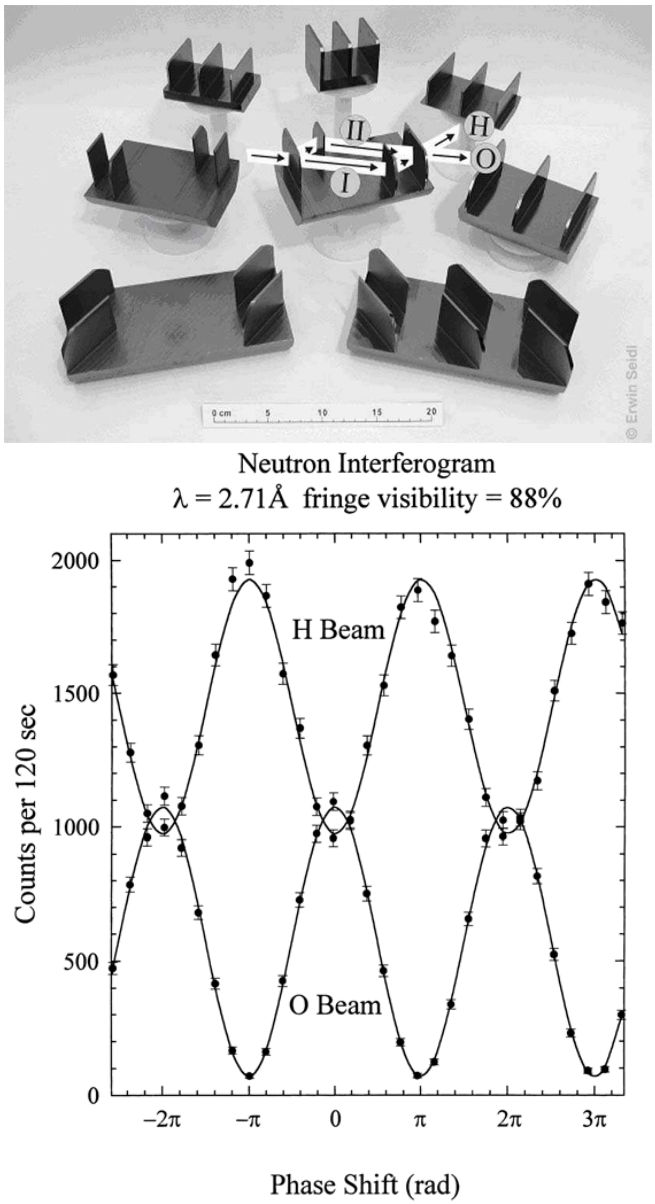

Fig. 1. Various perfect crystal neutron interferometers and a typical interference pattern

where b_c is the coherent scattering length, σ_r is the attenuation cross section, and N is the particle density of the phase shifting material. The different k-vector inside the phase shifter of thickness D causes a spatial shift $\vec{\Delta}$ of the wave packet, which depends on the orientation of the sample surface $\hat{s}$ and is related to the scalar phase shift χ by

$$\psi \to \psi_0 e^{i\vec{\Delta}\,\vec{k}} = \psi_0 e^{-iNb_c\lambda D} = \psi_0 e^{i\chi} \ , \tag{2}$$

where χ can be written as a path integral of the canonical momentum k_c along the beam paths $\chi = \oint \vec{k}_c d\vec{s}$ [11]. Therefore, the intensity behind the interferometer becomes

$$I_0 \propto \left|\psi_0^{\mathrm{I}} + \psi_0^{\mathrm{II}}\right|^2 \propto (1+\cos\chi) \ . \tag{3}$$

The intensity of the beam in the deviated direction I_H follows from the particle conservation ($I_0 + I_H = \mathrm{const}$). Thus, the intensities behind the interferometer vary as a function of the thickness D of the phase shifter, the particle density N, and the neutron wavelength λ.

Neutron optics is a part of quantum optics, and many phenomena can be described properly in that terminology, where the coherence function, which is the autocorrelation function of a wave function,

$$\Gamma(\vec{\Delta}) = \left\langle \psi(0)\psi(\vec{\Delta}) \right\rangle \ , \tag{4}$$

plays an important role [12, 13]. Using the wave packet description for the wave functions (amplitude $a(\vec{k})$)

$$\psi(\vec{x}) \propto \int a(\vec{k}) e^{i\vec{k}\,\vec{x}} dk \ , \tag{5}$$

one obtains

$$I_0(\vec{\delta}_0) \propto \left|\psi_0^{\mathrm{I}} + \psi_0^{\mathrm{II}}\right|^2 \propto 1 + \left|\Gamma(\vec{\Delta}_0)\right| \cos\chi_0 =$$

$$= 1 + |\Gamma(\Delta_0)| \cos(\vec{\Delta}_0\,\vec{k}_0) \ , \tag{6}$$

where $\vec{\Delta}_0$ and χ_0 denote the phase shifts at the mean momentum $\vec{k}_0$. This gives

$$\left|\Gamma(\vec{\Delta})\right| \propto \left| \int g(\vec{k}) e^{i\vec{k}\,\vec{\Delta}} d^3\vec{k} \right| \ . \tag{7}$$

One notices that, through $\Gamma(\Delta)$, each interference fringe is slightly different from any other, and this shows that each interference fringe has a distinct identity. The absolute value of the coherence function can be obtained from the fringe visibility $\left|\Gamma(\vec{\Delta})\right| = (I_{\mathrm{Max}} - I_{\mathrm{Min}})/(I_{\mathrm{Max}} + I_{\mathrm{Min}})$ or as the Fourier transform of the momentum distribution $g(\vec{k}) = \left|a(\vec{k})\right|^2$. The mean square distance related to $\left|\Gamma(\vec{\Delta})\right|$ defines the coherence length Δ_i^c, which is directly related for Gaussian distribution functions to the minimum uncertainty relation ($\Delta_i^c \delta k_i = 1/2$). Similar relations can be obtained for time-dependent phenomena, where the spectral distribution $g(\omega)$ and the temporal coherence function come into play.

T a b l e 1. Properties of neutrons

Particle Properties		Wave Properties
$m = 1.674928(1) \times 10^{-27}$ kg	Connection	$\lambda_c = \frac{h}{m.c} = 1.319695(20) \times 10^{-15}$ m
$s = \frac{1}{2}\hbar$ $\mu = -9.6491783(18) \times 10^{-27}$ J/T	de Broglie $\lambda_B = \frac{h}{m.v}$	for thermal neutrons: $\lambda = 1.8$ Å, $v = 2200$ m/s
$\tau = 887(2)$ s	Schrödinger	$\lambda_B = \frac{h}{m.v} = 1.8 \times 10^{-10}$ m
$R = 0.7$ m $\alpha = 120(2.5) \times 10^{-4}$ fm^3 $u - d - d$-quark structure	$H\psi(\vec{r},t) = i\hbar\frac{\delta\psi(\vec{r},t)}{\delta t}$ & boundary conditions	$\Delta_c = \frac{1}{2\delta k} \cong 10^{-8}$ m $\Delta_p = v.\Delta t \cong 10^{-2}$ m $\Delta_d = v.\tau = 1.942(5) \times 10^6$ m $0 \le \chi \le 2\pi(4\pi)$
m mass, s spin, μ magnetic moment, τ β-decay lifetime, R (magnetic) confinement radius, α electric polarizability; all other measured quantities like electric charge, magnetic monopole, and magnetic dipole moment are compatible width zero	$-\mu B$ ——— ↕ two lewel system μB ———	λ_c Compton wavelength, λ_B de Broglie wavelength, Δ_c coherence length, δ_p packet length, δk momentum width, Δt chopper opening time, v group velocity, χ phase

Any experimental device deviates from the idealized situations: the perfect crystal can have slight deviations from its perfectness, and its dimensions may vary slightly; the phase shifter contributes to such deviations by variations in its thickness and due to its inhomogeneities. Even the neutron beam itself contributes to a deviation from the idealized situation, because of its momentum spread δk. Therefore, the experimental interference patterns have to be described by a generalized relation

$$I \propto A + B\left|\Gamma(\vec{\Delta})\right| \cos(\chi + \Phi) \,, \tag{8}$$

where A, B, and Φ are characteristic parameters of a certain set-up. It should be mentioned, however, that the idealized behavior described by Eq. (3) can be approached by a well-balanced set-up (Fig. 1). Phase shifts can be applied in the longitudinal, transverse, and vertical directions, and the related coherence properties can be measured [14]. In the transverse direction, the phase shift becomes wavelength-independent ($\chi_T = -2d_{hkl}Nb_cD_0$; $d_{hkl}\ldots$ reflecting the lattice plane distance), which implies a much larger coherence length in that direction. All the results of interferometric measurements obtained up to now can be explained well in terms of the wave picture of quantum mechanics and the complementarity principle of standard quantum mechanics. Nevertheless, one should bear in mind that neutrons also carry well-defined particle properties, which have to be transferred through the interferometer. These properties are summarized in Table 1 together with a formulation in the wave picture. Both particle and wave properties are well established, and, therefore, neutrons seem to be a proper tool for testing quantum mechanics with massive particles, where the wave-particle dualism becomes very obvious.

All neutron interferometric experiments pertain to the case of self-interference, where only one neutron is inside the interferometer during a certain time interval, if at all. Usually, at that time, the next neutron has not yet been born and is still contained in the uranium nuclei of the reactor fuel. Although there is no interaction between different neutrons, they have a certain common history within predetermined limits, which are defined, e.g., by the neutron moderation process, by their movement along the neutron guide tubes, by the monochromator crystal, and by the special interferometer set-up. Therefore, any interferometer pattern contains single-particle and ensemble properties together.

2. Classic Neutron Interference Experiments

Here, only short comments to these experiments are given, since at least some of them provide the basis of the more recent investigation described in the following sections. More details can be found in a related book [5].

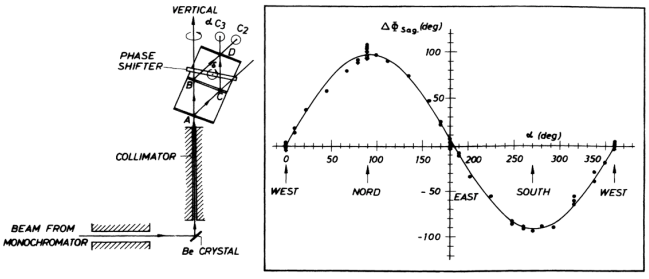

Fig. 2. Results of the neutron interferometric Earth rotation experiment [16, 17]

2.1. Gravity experiments

The gravitational interaction of neutrons is under usual laboratory conditions of the same order of magnitude as the mean nuclear and magnetic interaction, and, therefore, a measurable interference signal is to be expected. The interaction Hamiltonian in this case reads

$$H_g = m\vec{g}\vec{r} - \vec{\omega}\hbar(\vec{r} \times \vec{k}) \,, \tag{9}$$

where $\vec{g}$ means the gravitational acceleration directed toward the center of the Earth, and $\vec{\omega}$ is the angular rotation frequency of the Earth.

The phase shift within the interferometer is calculated, by using the path integral with the canonical momentum, as mentioned earlier. In this way, after several intermediate steps, one gets the *gravitational phase shift*

$$\beta = \frac{m^2 g\lambda A \sin\Phi}{2\pi\hbar^2} + \frac{2m\omega A \sin\phi_L \sin\varepsilon}{\hbar} \,, \tag{10}$$

where A is the area enclosed by the coherent beam trajectories in the interferometer, Φ is the angle, at which the interferometer is turned out of the horizontal plane, Φ_L is the latitude of the point, at which the experiment takes place, and ε is the angle of rotation around the vertical axis. The first expression in the above equation describes the familiar gravitational term and has been proven by Colella, Overhauser, and Werner [15] by rotating the interferometer around a horizontal axis (*COW-experiment*). This phase shift can be understood as the effect of the different gravitational potentials of the two coherent beams, as one travels higher within the potential than the other one. The *Coriolis or Sagnac term* in Eq. (9) has first been observed experimentally by Werner *et al.* [16, 17] by directing a neutron beam vertically upward and by turning a perfect crystal interferometer around this vertical axis (see Fig. 2).

The result gives impression of how sensitive the interferometric measuring method actually is. The easiest way to visualize this effect is by imagining the area encompassed by the two coherent beams as a differently oriented flag on the rotating Earth. A more detailed discussion can be found in [18].

A complimentary investigation to the gravitational measurements was performed by Bonse and Wroblewski [19], when they put the interferometer in an oscillatory motion and, in so doing, also observed a phase shift, being proportional to the respective acceleration of the interferometer plates. In summary, this proved the validity of the classical transformation laws for *non-inertial frames of reference* in the quantum limit. Using moving phase shifters, the neutron Fizeau effect has been observed as well [20, 21]. For matter waves, the Fizeau effect depends on the velocity of the surface and not on the motion of the bulk, as in the case of electromagnetic waves.

2.2. 4π-Spinor symmetry

This is probably one of the most intensively discussed interference experiments done with matter waves. Based on the elementary principles of quantum mechanics, the propagation of a wave function can be described by a unitary transformation, given by the relevant Hamiltonian. For the magnetic interaction, $H_m = -\vec{\mu}\vec{B}$, the propagation of the two-component *spinor wave function*, which describes the neutron as a fermion, can be represented as follows:

$$\psi(t) = e^{iHt/\hbar}\psi(0) = e^{-i\vec{\mu}\vec{B}t/\hbar}\psi(0) =$$

$$= e^{-i\vec{\sigma}\vec{\alpha}/2}\psi(0) = \psi(\alpha) \,, \tag{11}$$

where α means the *Larmor precession angle*

$$|\alpha| = \frac{2\mu}{\hbar}\int Bdt = \frac{2\mu}{\hbar v}\int Bds \,. \tag{12}$$

When inserting the Pauli spin operators, one can easily show that $\psi(\alpha)$ has a 4π-*symmetry* and not the 2π-symmetry, which we should use with respect to expectation values and within the scope of classical physics,

$$\begin{aligned} &\psi(2\pi) = -\psi(0) \,, \\ &\psi(4\pi) = \psi(0) \,. \end{aligned} \tag{13}$$

These facts, which were not previously regarded as verifiable, can be elucidated very easily with neutron interferometry by observing the intensity modulations, while

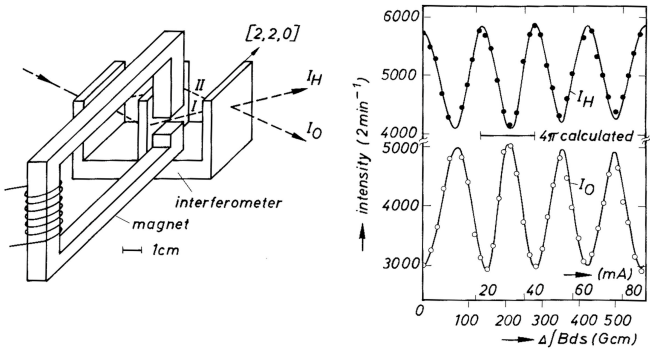

Fig. 3. Results of the neutron interferometric 4π experiment [22]

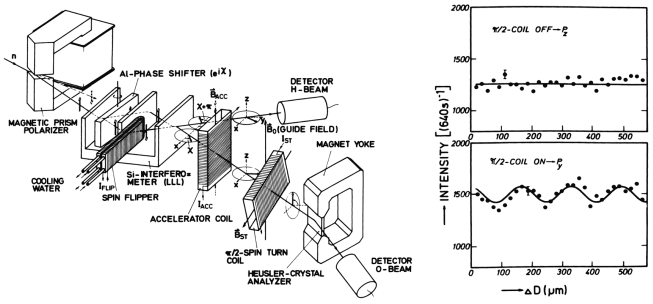

Fig. 4. Sketch of the experimental set-up and typical results of the spin-superposition experiment [25]

one of the coherent beams passes through a magnetic field,

$$I_0 = |\psi_0(0) + \psi_0(\alpha)|^2 \propto \left(1 + \cos\frac{\alpha}{2}\right) . \tag{14}$$

The above relations are valid for polarized as well as for unpolarized neutrons, which points to the inherent symmetry properties of fermions. From Eqs. (13) and (14), one recognizes that the original state is reproduced only for $\alpha = 4\pi$. This was verified, nearly simultaneously, in measurements by Rauch *et al.* [22] and by Werner *et al.* [23]. Afterward, this effect was also proven through several other methods and for a series of other fermion systems. A distinction between dynamical and topological phases will be discussed in Section 4.

2.3. Spin-superposition

Spin superposition is a frequently used principle of quantum mechanics. Its curiosity value has been stressed by Wigner [24]. The wave function of both coherent beams is originally polarized in the $|z\rangle$-direction. One beam is then inverted to a polarization in the $|-z\rangle$-direction, whereas the other remains unchanged. Both beams are then superimposed. This spin flip can be produced, for example, by the Larmor precession around a magnetic field perpendicular to the z-direction. If we also allow for a nuclear phase shift, one gets

$$\psi(\chi,\pi) = e^{1\chi} e^{-i\sigma_y \pi/2} |+z\rangle = -i\pi\sigma_y e^{i\chi} |+z\rangle =$$

$$= e^{i\chi} \big|-z\big\rangle . \tag{15}$$

The total wave function $\psi = |+z\rangle + e^{i\chi}|-z\rangle$ leads to the following intensity and polarization of the out-going beam $I = \text{const}$:

$$\vec{p} = \frac{\psi^* \vec{\sigma} \psi}{\psi^* \psi} = \begin{pmatrix} \cos\chi \\ \sin\chi \\ 0 \end{pmatrix} . \tag{16}$$

Thus, the intensity does not show any dependence on the phase shift, but the polarization shows a marked χ dependence, where the polarization vector lies in the x, y-plane and is perpendicular to the polarizations of the two superimposed coherent beams. The results of a related experiment are shown in Fig. 4. This implies that a pure quantum state in the $|z\rangle$-direction, e.g. for $\chi = 0$, has been transformed into a quantum state in the $|x\rangle$-direction. In the sense of self-interference, which definitively applies here, it seems that each neutron has information about the physical situation in both of the widely separated coherent beams. The experiment by Summhammer *et al.* [25] has fully confirmed this process. Intensity modulations appear only when the polarization analysis is done in the x, y-plane. This becomes relevant in a recent experiment concerning the contextuality problem in quantum physics (see Section 5).

The experiment mentioned above has been repeated with a *Rabi resonance flipper*, which is also routinely used as a spin-flipping device in polarized neutron physics. Along with the spin flip, a simultaneous energy exchange takes place between the resonator system and the neutrons, as it has been described by Drabkin and Zhitnikov [26] and tested experimentally by Alefeld *et al.* [27] ($\Delta E = \hbar\omega_r = 2\mu B_0$, where B_0 is the strength of the guide field). Here, one has to use the time-dependent Schrödinger equation and to consider the exchange of the total energy of the neutron system

$$\psi(\chi,\omega_r) = e^{i\chi} e^{-i(\omega-\omega_r)t} \big|-z\big\rangle , \tag{17}$$

which leads to the following polarization, when the other unchanged coherent beam $|z\rangle$ is superimposed,

$$\vec{p} = \begin{pmatrix} \cos(\chi - \omega_r t) \\ \sin(\chi - \omega_r t) \\ 0 \end{pmatrix} . \tag{18}$$

The polarization is also in the x, y-plane. However, it rotates within this plane synchronously with the resonance

flip-field. It was possible to demonstrate this effect with a stroboscopic measurement, where the polarization in a given direction was measured synchronously with the phase of the flip-field [28].

In connection with these results, the obvious question arises whether the measurement of the energy transfer makes a determination of the beam path possible. One can, however, show that this is impossible, because the interference vanishes in the presence of a measurable energy shift (i.e. larger than the energy width of the beam), and because the measurement of the energy change of the flip-field is impossible due to the *photon number-phase uncertainty relationship* ($\delta\phi\delta N > 1$).

These energy exchange measurements have been extended by Summhammer *et al.* [29] to multiphoton exchange experiments. In this case, the off-resonance oscillating magnetic field with a frequency of 7.534 kHz was inserted into one beam, and up to five photon emission and absorption processes have been identified from the time-resolved interference pattern.

2.4. Neutron Josephson effect

A double coil arrangement can be used for the observation of a new quantum beat effect, which is the magnetic analog to the well-known superconducting electric Josephson effect. If the frequencies of the two flipper coils are chosen to be slightly different, the energy transfer becomes different too ($\Delta E = \hbar(\omega_{r1} - \omega_{r2})$. The flipping efficiencies for both coils are very close to 1 (better than 99%). Now, the wave functions change accordingly to

$$\psi \to e^{i(\omega-\omega_{r1})t}\left|\downarrow\right\rangle + e^{i\chi}e^{i(\omega-\omega_{r2})t}\left|\downarrow\right\rangle . \tag{19}$$

Therefore, the intensity behind the interferometer exhibits a typical quantum beat effect given by

$$I \propto 1 + \cos\left[\chi + (\omega_{r1} - \omega_{r2})t\right] . \tag{20}$$

Thus, the intensity behind the interferometer oscillates between the forward and deviated beams without any apparent change inside the interferometer [32]. The time constant of this modulation can reach a macroscopic scale (in our case, 50 s), which is correlated to the uncertainty relation $\delta E\Delta t \leq \hbar/2$. This relates to an energy sensitivity of 2.7×10^{-19} eV, which is many orders of magnitudes better than that of other advanced spectroscopic methods. This high resolution is strongly decoupled from the monochromaticity of the neutron beam, which was $\delta E_B = 5.5 \times 10^{-4}$ eV around a mean energy of the beam $E_B = 0.023$ eV in this case. The quantum beat effect can also be interpreted as the magnetic Josephson effect analog, where the phase difference $\Delta(t)$ is driven by the magnetic energy, whereas, in the well-known Josephson effect in superconducting tunnel junctions [33], the phase of the Cooper pairs in both superconductors is driven by the electrical energy.

2.5. Stochastic versus deterministic beam path detection

A certain beam attenuation can be achieved either by a semitransparent material or by a proper chopper or slit system. The transmission probability is defined, in the first case, by the attenuation cross section σ_a of the phase shifting material [$\underline{a} = I/I_0 = \exp(-\sigma_a N\, D)$]. The change of the wave function is obtained directly from the complex index of refraction (Eq. (1)):

$$\psi \to \psi_0 e^{i(n-1)kD} = \psi_0 e^{i\chi} e^{-\sigma_a ND/2} = e^{i\chi}\sqrt{\underline{a}}\psi . \tag{21}$$

Therefore, the beam modulation behind the interferometer is obtained in the form

$$I_0 \propto \left|\psi_0^{\mathrm{I}} + \psi_0^{\mathrm{II}}\right|^2 \propto \left[(1+a) + 2\sqrt{\underline{a}}\cos\chi\right] . \tag{22}$$

On the other hand, the transmission probability of a chopper wheel or another shutter system is given by the open-to-closed ratio, $t = t_{\mathrm{open}}/(t_{\mathrm{open}} + t_{\mathrm{closed}})$, and one obtains after straightforward calculations

$$I \propto \left[(1-\underline{a})\left|\psi_0^{\mathrm{II}}\right|^2 + \underline{a}\left|\psi_0^{\mathrm{I}} + \psi_0^{\mathrm{II}}\right|^2\right] \propto$$

$$\propto \left[(1+\underline{a}) + 2\underline{a}\cos\chi\right] , \tag{23}$$

i.e. the contrast of the interference pattern is proportional to $\sqrt{\underline{a}}$ in the first case and to a in the second case, although the same number of neutrons are absorbed in both cases. The absorption represents a measuring process in both cases, i.e. a beam path detection, because compound nuclei are produced with an excitation energy of several MeV, which are usually deexcited by capture gamma rays. The measured contrast verifies the "stochastic" and "deterministic" predictions (Eqs. 22 and 23) [32, 33]. The different contrast becomes especially obvious for low transmission probabilities. The discrepancy diverges for $\underline{a} \to 0$, but it has been shown that, in this regime, the variations of the transmission due to variations of the thickness or the density of the absorber plate have to be taken into account, which shifts the points below the $\sqrt{\underline{a}}$- ("stochastic") curve [34]. The region between a linear and a square root behavior can be reached by very narrow chopper slits or by narrow transmission lattices, where

one starts to loose information of through which individual slit the neutron went. This is exactly the region which shows the transition between a deterministic and a stochastic situation and, therefore, it can be formulated by a Bell- like inequality ($\sqrt{\underline{a}} > x > \underline{a}$ [35]).

The stochastic limit corresponds to the quantum limit when one does not know anymore through which individual slit the neutron went. Which situation exists depends on how the slit widths l compare to the coherence lengths in the related direction. In case that the slit widths become comparable to the coherence lengths, the wave function behind the slits shows distinct diffraction peaks which correspond to new quantum states ($n \neq 0$). The creation of the new quantum states means that those labelled neutrons carry information about the chosen beam path and, therefore, do not contribute to the interference amplitude [36] (Fig. 5). A related experiment has been carried out by rotating an absorption lattice around the beam axis, where one changes from $l \ll \Delta_x^c$ (vertical slits) to $l \gg \Delta_y^c$ (horizontal slits). Thus, the attenuation factor $\underline{a}$ has to be generalized including not only nuclear absorption and scattering processes but also lattice diffraction effects, if they remove neutrons from the original phase space.

The partial absorption and coherence experiments are closely connected to the quantum duality principle which states that the observation of an interference pattern and the acquisition of which-way information are mutually exclusive. Various inequalities have been formulated to describe this mutual exclusion principle [37–39]. The most concise formulation reads

$$V^2 + P^2 =\leq 1 \,, \tag{24}$$

where V denotes the fringe visibility (Eq. (5)), and P is the predictability of the path through the interferometer, which is a quantitative measure of the *a priori* which-way knowledge.

3. Post-Selection Experiments

Various post-selection measurements in neutron interferometry have shown that interference fringes can be restored by proper filtering methods even in cases where the overall beam does not exhibit any interference fringes due to spatial phase shifts larger than the coherence lengths of the interfering beams [40, 41]. Post-selection procedures can be applied to various parameters of an experiment:

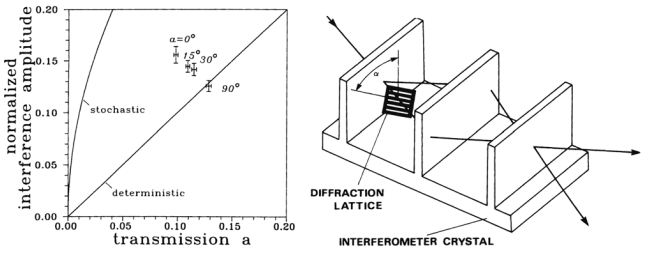

Fig. 5. Lattice absorber in the interferometer approaching the classical limit, when the slits are oriented horizontally, and the quantum limit, when they are oriented vertically [36]

- spatial post-selection
- momentum post-selection
- counting statistic post-selection
- phase post-selection
- topology post-selection

Figure 6 shows some of them schematically. Here, we discuss the momentum post-selection and phase phase-echo experiments. For other methods, we refer the reader to the literature [42, 43].

3.1. Post-selection of momentum states

The experimental arrangement with the indication of the wave packets at different parts of the interference experiment is shown in Fig. 6. An additional monochromatization is applied behind the interferometer by means of the Bragg diffraction from single crystals or by time-of-flight systems. The momentum-dependent intensity for Gaussian momentum distributions reads

$$I_0(k) = \exp[-(k-k_0)^2/2\delta k^2] \left\{ 1 + \cos\left(\chi_0 \frac{k_0}{k} \right) \right\} \,. \tag{25}$$

The spatial phase shift-dependent intensity is given by Eq. (6). The formula shows that the overall interference fringes disappear for spatial phase shifts much larger than the coherence lengths [$\delta_i \geq \delta_i^c = 1/(2\delta k_i)$]. The surprising feature is that $I_0(k)$ becomes oscillatory for large phase shifts, where the interference fringes described by Eq. (5) disappear ([38], see Fig. 7). This indicates that the interference in the phase space has to be considered [44]. The amplitude function of the packets arising from beam paths I and II determines the spatial shape of the packets behind the interferometer,

$$I_0(x) = |\psi(x) + \psi(x+\delta)|^2 \,, \tag{26}$$

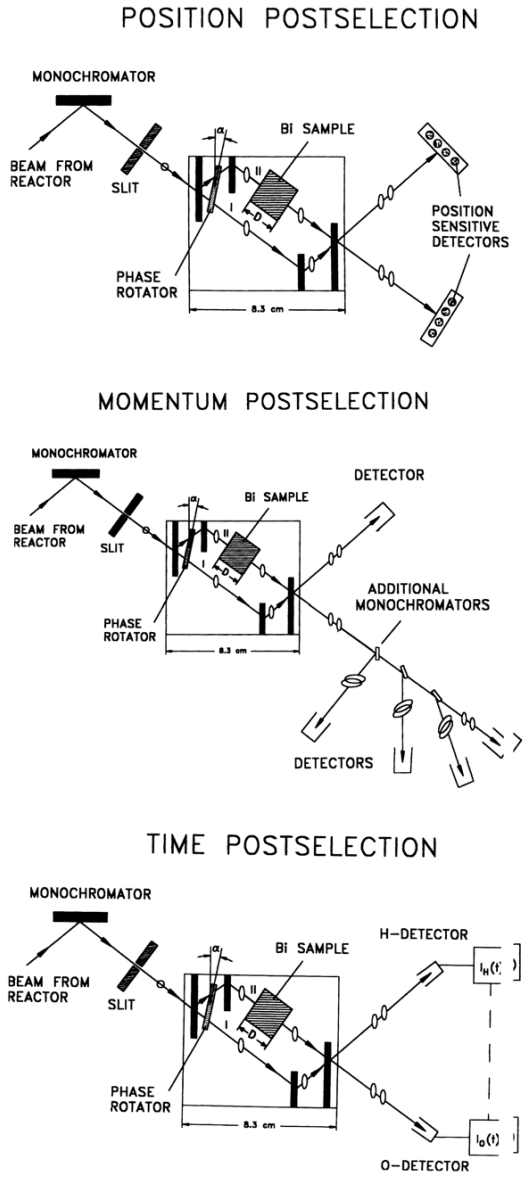

Fig. 6. Sketch of various post-selection methods with an indication of the related wave packets

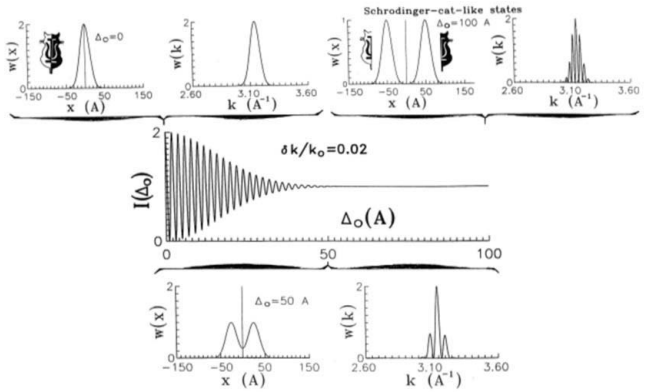

Fig. 7. Interference pattern as a function of the relative phase shift (middle) and related wave packets and momentum spectra behind the interferometer for different values of the phase shift [40]

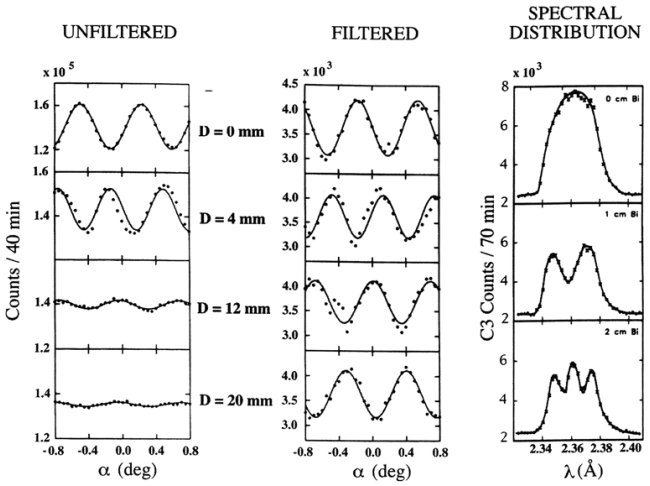

Fig. 8. Interference pattern of the unfiltered overall beam ($dk/k_0 = 0.012$, middle) and the filtered beam reflected from a nearly perfect crystal analyzer in the antiparallel position ($dk'/k_0 = 0.0003$, left), and the observed spectral modulation (right) of the outgoing beam for different phase shifter thicknesses [41]. These measurements have been done with a set-up shown in the middle of Fig. 6

which separates for large phase shifts into two peaks (Fig. 7).

For an appropriately large displacement ($\Delta \gg \Delta^c$), the related state can be interpreted as a superposition state of two macroscopically distinguishable states, that is a stationary Schrödinger cat-like state [43, 44], but here first for massive particles. These states – separated in the ordinary space and oscillating in the momentum space – seem to be notoriously fragile and sensitive to dephasing and de-coherence effects [45–50].

Measurements of the wavelength (momentum) spectrum were made with an additional silicon crystal placed behind the interferometer with a rather narrow mosaic spread (high resolution), which reflects, in the parallel position, a rather narrow band of neutrons only ($\delta k'/k_0 \approx 0.0003$) causing a restored visibility even at large phase shifts [41] (Fig. 8). This feature shows that an interference pattern can be revived even behind the interferometer by means of a proper post-selection procedure. In this case, the overall beam does not show interference fringes anymore, and the wave packets originating from the two different beam paths do not over-

lap. The momentum distribution has been measured by scanning the analyzer crystal through the Bragg position. These results clearly demonstrate that the predicted spectral modulation (Eq. (25)) appears, when the interference fringes of the overall beam disappear. The modulation is somehow smeared out due to averaging processes across the beam due to various imperfections, unavoidably existing in any experimental arrangement. The contrast of the empty interferometer was 60%.

The new quantum states created behind the interferometer can be analyzed with regard to their uncertainty properties. Analogies between a coherent state behavior and a free but coherently coupled particle motion inside the interferometer have been addressed [31]. In such cases, the dynamical conjugate variables x and p minimize the uncertainty product with identical uncertainties $(\Delta x)^2 = (\Delta k)^2 = 1/2$ (in dimensionless units). Simple calculations show that, for $(\Delta k)^2$, a value below the coherent state value can be achieved, which means the squeezing in quantum optic terminology [49–54]. One emphasizes that a single coherent state does not exhibit the squeezing, but a state created by the superposition of two coherent states can exhibit a considerable amount of squeezing. Thus, highly non-classical states are made by the power of the quantum mechanical superposition principle.

It should be mentioned that the momentum post-selection in typical Bell experiments (EPR-experiments) with entangled photons may also give a less mystic view about these experiments, since more information can be extracted, when the momentum post-selection is added [40].

General conclusions about wave function properties can only be drawn if all accessible information about it is included. Thus, the completeness of a quantum experiment has to be seen in a new light. The non-locality phenomenon of quantum mechanics can be understood as the far reaching action of the plane wave components of the wave function as well. The band width is determined by the momentum resolution of the measurement with an upper limit defined by the inverse of the source-detector distance.

3.2. Contrast retrieval by phase-echo

A large phase shift ($\Delta > \Delta^c$) can be applied in one arm of the interferometer, which can be compensated by a negative phase shift acting in the same arm or by the same phase shift applied to the second beam path [55]. Because the phase shift is additive, the coherence function depends on the net phase shift only. Thus, the interference pattern can be restored, as it is shown, in the form of an experimental example in Fig. 9. The phase-echo method can also be applied behind the interferometer loop when multiplate interferometers are used [43]. In this case, the situation becomes even more similar to the situation discussed in the previous section. The experimental results completely confirmed that behavior. Phase echo is a technique similar to spin echo [3], which is routinely used in neutron spectroscopy and represents an interference experiment as well.

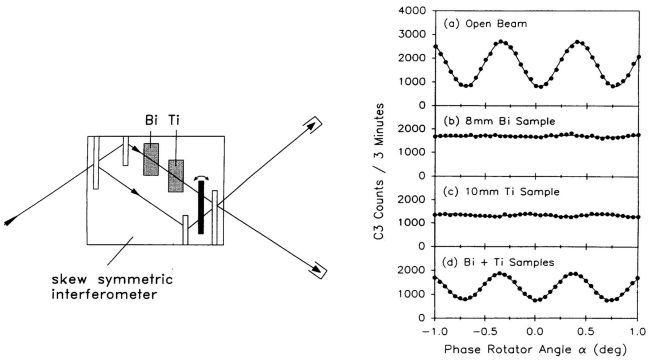

Fig. 9. Loss of contrast at high interference and its retrieval by an opposite phase shifter inserted into the same beam [55]

Nevertheless, it should be mentioned that a complete retrieval seems to be impossible due to theoretical and practical limitations [56, 57].

4. Topological Effects

Topological and geometric effects appear in the solution of the Schrödinger equation due to special geometric forms of the interaction [58–60]. Thus, they are a part of quantum mechanics, but they are easily overlooked by pure intensity experiments. It also shows that a wave-function often carries more information than that extracted in a standard experiment. A typical example is the spin superposition experiment discussed in Section 2.3, where the result also depends around which axis the spin has been rotated into the opposite direction. In this respect, the action of a Hamiltonian can be separated into a part related to its strength (dynamical) and its geometry, which results from the sum of state changes along the excursion in the phase space

$$\phi = -\frac{1}{\hbar}\int_0^T \langle\psi(t)|\mathcal{H}|\psi(t)\rangle dt +$$

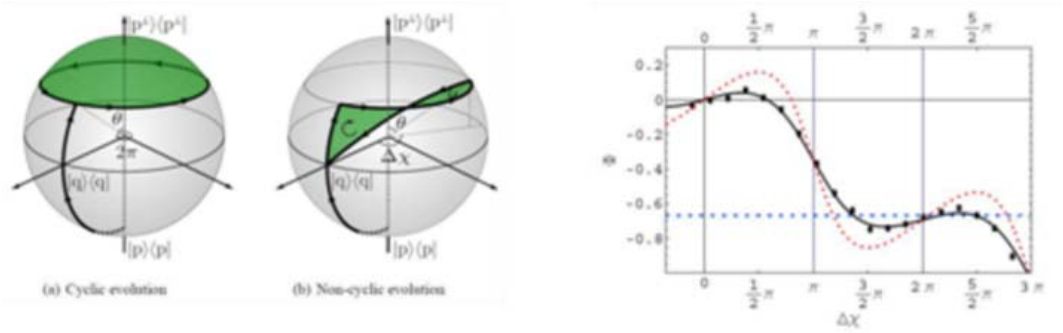

Fig. 10. Diagonal and off-diagonal geometric phases drawn on Poincaré spheres and the results for a non-adiabatic non- cyclic excursion measurement [68]

$$+i\int_0^T \left\langle \phi(t)\frac{d}{dt}\middle|\phi(t)\right\rangle dt = \alpha + \phi_g \ , \tag{27}$$

with $\left|\phi(t) \geq e^{i\phi}\right| \psi(t)\rangle$.

Wagh *et al.* [61] did recently a related experiment and showed clearly the existence of the topological phase. In a similar sense, the scalar and vector *Aharonov–Bohm effects* of neutrons have been verified by neutron interferometric methods [62, 63]. In the case of an adiabatic excursion, the geometric phase becomes half the solid angle of the excursion seen on the Bloch sphere

$$\phi_g = -\frac{\Omega}{2} \ . \tag{28}$$

This has been verified recently with a high accuracy with ultra-cold neutrons guided by slowly varying magnetic fields $\phi_g = -0.51(1)\Omega$ [64]. Off-diagonal and non-adiabatic geometric phases have been predicted as well [60, 65]. Detailed proposals and related experiments have been done [66, 67]. In the Poincaré representation, the diagonal phases are given by the solid angle opened up by the excursion line $|\psi_i$ to $|\psi_f\rangle$ and their geodesies to the pole, whereas off-diagonal phases are given by two excursion lines and their connection line in form of geodesies. In a related experiment, the non-adiabatic and non-cyclic phases have been verified with a double-loop interferometer, where two phase shifters (PS) and an absorber (A) permit quite peculiar state excursions, as shown in Fig. 10 [68].

It should be mentioned that just geometric phases show a high robustness against the fluctuation and dissipative effects, as predicted by DeChiara and Palma [69] and verified experimentally by Filipp *et al.* [64]. This may have remarkable consequences for quantum communication systems.

5. Quantum Contextuality

A. Einstein, B. Podolsky, and N. Rosen [70] argued that quantum mechanics may not be complete, since non-local correlations between spatially separated systems are predicted, which stimulated the discussion about "hidden" variables and a more "realistic" theory. J. Bell [35] formulated inequalities which can destinguish between the quantum mechanical and the "realistic" view [71, 72]. Related experiments with entangled photons verified the non-local view of quantum mechanics [73–76]. Entanglement does not exist between two particles (photons) only, but also between different degrees of freedom of a single system (neutron). This yields the concept of "contextuality", which states that independent measurements of independent observables are correlated. In our case, the beam path through the interferometer and the spin states are taken as independent observables. In this case, a Bell-like inequality can be formulated, which can be measured from the counting rates N at different values of the phase shift χ and the spin rotation angle α [67]:

$$-2 \leq S \leq 2 \ ,$$

$$S = E(\alpha_1, \chi_1) + E(\alpha_1, \chi_2) - E(\alpha_2, \chi_1) + E(\alpha_2, \chi_2) \ ,$$

$$E(\alpha, \chi) =$$

$$= \frac{N(\alpha,\chi)+N(\alpha+\pi,\chi+\pi)-N(\alpha,\chi+\pi)-N(\alpha+\pi,\chi)}{N(\alpha,\chi)+N(\alpha+\pi,\chi+\pi)+N(\alpha,\chi+\pi)+N(\alpha+\pi,\chi)}. \tag{29}$$

The maximal violation of this inequality due to quantum mechanics happens for the parameters $\alpha_1 = 0$, $\alpha_2 = \pi/2$,

$\chi_1 = \pi/4$, and $\chi_2 = -\pi/4$ and amounts to $S = 2\sqrt{2} = 2.82$.

The measurement scheme is shown in Fig. 11. The entangled neutron state has been produced by rotating the neutron spin in beam path I into the $|-y>$ and in beam path II into the $|y>$ direction, respectively. The precise determination of the related counting rates at the parameter values given above yielded the following value for S [67]:

$$S = 2.051 \pm 0.019 \,,$$

which is by a 3σ-limit above 2, verifying the contextuality principle of quantum mechanics for the first time.

The maximal violation of $S = 2.82$ has not been achieved, because the contrast of the interference pattern and the neutron polarization were below 1. In this kind of measurements, these quantities play a similar role as the finite efficiency of the photon detectors in entangled photon experiments. In a subsequent and improved experiment, a violation up to $S = 2.291 \pm 0.008$ has been measured [77].

The same set-up, as shown in Fig. 11, has been used to perform experiments related to the Kochen–Specker theorem [78] and the Mermin inequalities [79], where even stronger violations of classical hidden variable theories can be verified. For neutron matter-waves, a related proposal came from Basu *et al.* [66]. A related experiment has been performed using a set-up similar to that shown in Fig. 11, but with the additional feature that the beam paths could be closed alternatively by means of an absorber sheet [80]. The measurement of the product observable $(\sigma_x^s\sigma_v^p)(\sigma_v^s\sigma_x^p)$ was done by measuring $(\sigma_z^s\sigma_z^p)$ and using *a priori* the non-contextuality relation. The measurable quantity is defined by a sum of product observables

$$C = \hat{I} - \sigma_x^s\sigma_x^p - \sigma_y^s\sigma_y^p - (\sigma_x^s\sigma_y^p)\,(\sigma_y^s\sigma_x^p) \,. \tag{30}$$

In any experiment, the expectation values only can be measured. For non-contextual models, the last term can be separated:

$$\langle(\sigma_x^s\sigma_y^p)\rangle\langle(\sigma_y^s\sigma_y^p)\rangle = \langle\sigma_x^s\rangle\langle\sigma_y^p\rangle\langle\sigma_y^s\rangle\langle\sigma_y^p\rangle \,, \tag{31}$$

which gives

$$C_{nc} = \pm 2 \,, \tag{32}$$

whereas quantum mechanics predicts

$$C_{qm} = 4 \,. \tag{33}$$

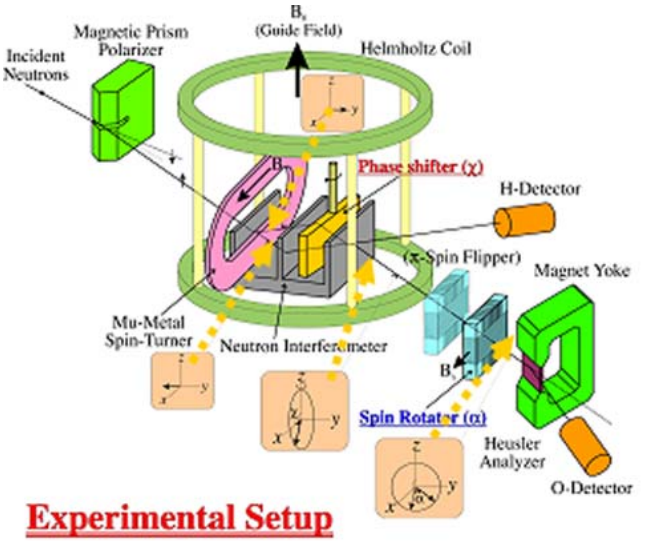

Fig. 11. Sketch of the experimental set-up for the contextuality experiment. The phase χ and the polarization rotation α could be varied independently [67]

The measured value was

$$C_{\rm exp} = 3.138 \pm 0.0115 \,, \tag{34}$$

which is well above the non-contextuality (classical) limit of 2 and provides an all-versus-nothing-type contradiction. It is also a Peres–Mermin proof of quantum-mechanics against non-contextual hidden variable theories.

A debate in the literature [81, 82] criticized the *a priori* use of the non-contextuality relation $(\sigma_x^s\sigma_y^p)\,(\sigma_y^s\sigma_x^p) = (\sigma_z^s\sigma_z^p)$ and, in this connection, the use of an absorber to measure this quantity. In the follow-up proposal [83] and the subsequent experiment [77], the previous result (Eq. 34) has been verified, and an even stronger violation has been observed. In this case, a quantum erasure has been used instead of an absorber, and, therefore, all quantities required for Eq. (34) could be measured within the same context.

Years ago, it has been shown that the Zeeman energy ($\hbar\omega = 2\mu B_n$) can be exchanged between the neutron and a resonance coil coherently [27]. This provides the basis for triple entanglement experiments using spin-path-energy as independent degrees of freedom [84]. These GHz-states are a new tool for basic neutron quantum optics experiments and may be new components of quantum computing elements like C-NOT gates. The energy states have geometric nature and may be rather robust under dissipative effects, as shown in [64].

6. Discussion

It has been shown that more information about a quantum system can be extracted, when more accessible parameters are measured, i.e. when post-selection methods are applied. It becomes obvious that a system may remain coupled in the phase space, even when it becomes separated in any other parameter space. Thus, interference properties can be shifted from one parameter space to another one and back again. Related bands of plane wave components, which compose the wave packets, may be considered as a responsible factor for the understanding of the coupling and non-locality phenomena in quantum mechanics. It looks like that these plane wave components of the wave packets, i.e. narrow bands, interact over much larger distances than the size of the overall packets. This interaction guides neutrons of certain momentum bands to the 0- or H-beam, respectively. These phenomena throw a new light on the discussion on Schrödinger-cat-like situations in quantum mechanics [70, 71]. It may be considered as a contribution to speakable and unspeakable aspects of quantum mechanics [72]. Spatially separated packets remain entangled (correlated) in the phase space, and non-locality appears as a result of this entanglement. The analogy with optical experiments performed in the time-frequency domain is striking [76]. Since the entanglement exists not only between objects but also between different degrees of freedom, Bell-type experiments can also be done in single particle experiments [66]. In this respect, contextuality experiments with neutrons (Section 5) may be of special value, since they show that the experimental outcome when measuring the commuting observables (spin and beam path) are intrinsically correlated, and the quantum contextuality may be considered as an important feature of quantum physics. This also shows that the quantum systems contain stronger correlations than classical ones, and contextuality may cause an additional loophole for the deviation of Bell inequalities [85].

The summaries drawn for the different experimental situations discussed in this article are followed by statements that the retrieval of the interference properties by several post-selection procedures became increasingly more difficult, the wider the separation in any parameter space of the quantum system happened before. This is caused by fluctuations, which are unavoidable due to residual quantum fluctuations inherent to any physical system.

Unavoidable fluctuations (even zero-point fluctuations) cause the irreversibility effect, which becomes more influential for widely separated Schrödinger-cat like states. All these effects can be described by an increasing entropy inherently associated with any kind of interaction. This also supports the idea of that the irreversibility is a fundamental property of the Nature, and the reversibility is an approximation only, as stated by several authors [86-89].

All the results of the neutron interferometric experiments are well described by the formalism of quantum mechanics. According to the complementarity principle of the Copenhagen interpretation, the wave picture has to be used to describe the observed phenomena. The question how the well-defined particle properties of a neutron are transferred through the interferometer is not a meaningful one within this interpretation, but, from the physical point of view, it should be an allowed one.

More complete quantum experiments show that a complete retrieval of all wave components behind an interaction the quantum system experienced becomes impossible, in principle. This implies, on a high accuracy level, a basic non-commutativity of operators $A.B|\psi\rangle \neq B.A|\psi\rangle$.

Most of the experimental work has been supported by projects of the Austrian Science Foundation (FWF), most recently by the project P 18943-N20. All coworkers mentioned in the self-citations are gratefully acknowledged.

1. H. Maier-Leibnitz and T. Springer, Z. Physik **167**, 386 (1962).
2. H. Rauch, W. Treimer, and U. Bonse, Phys. Lett. A **47**, 369 (1974).
3. F. Mezei, Z. Physik **25**, 146 (1972).
4. A.I. Ioffe, V.S. Zabiyankan, and G.M. Drabkin, Phys. Lett. **111**, 373 (1985).
5. H. Rauch and S.A. Werner, *Neutron Interferometry* (Clarendon Press, Oxford, 2000).
6. U. Bonse, and M. Hart, Appl. Phys. Lett. **6**, 155 (1965).
7. W. Bauspiess, U. Bonse, and W. Graeff, J. Appl. Cryst. **9**, 68 (1976).
8. H. Rauch and D. Petrascheck, in *Neutron Diffraction*, edited by H. Dachs, (Springer, Berlin, 1978), p. 303.
9. M.L. Goldberger and F. Seitz, Phys. Rev. **71**, 294 (1947).
10. V.F. Sears, *Neutron Optics* (Oxford Univ. Press, 1989).
11. R.P. Feynman, R.B. Leighton, and M. Sands, *The Feynman Lectures on Physics* (Addison-Wesley, New York, 1965), Vol. III.
12. R.J. Glauber, Phys. Rev. **130**, 2529; **131**, 2766 (1963).
13. L. Mandel and E. Wolf, *Optical Coherence and Quantum Optics* (Cambridge Univ. Press, Cambridge, 1995).

14. H. Rauch, H. Wlwitsch, H. Kaiser, R. Clothier, and S.A. Werner, Phys. Rev. A **53**, 902 (1996).
15. R. Colella, A.W. Overhauser, and S.A. Werner, Phys. Rev. Lett. **34**, 1472 (1975).
16. S.A. Werner, J.L. Staudenmann, and R. Colella, Phys. Rev. Lett. **42**, 1103 (1979).
17. J.L. Staudenmann, S.A. Werner, R. Colella, and A.W. Overhauser, Phys. Rev. A **21**, 1419 (1980).
18. D.M. Greenberger, Rev. Mod. Phys. **55**, 875 (1983).
19. U. Bonse and T. Wroblewski, Phys. Rev. Lett. **51**, 1401 (1983).
20. M.A. Horne, A. Zeilinger, A.G. Klein, and G.I. Opat, Phys. Rev. A **28**, 1 (1983).
21. A.G. Klein, G.I. Opat, A. Cimmino, A. Zeilinger, W. Treimer, and R. Gähler, Phys. Rev. Lett. **46**, 1551 (1981).
22. H. Rauch, A. Zeilinger, G. Badurek, A. Wilfing, W. Bauspiess, and U. Bonse, Phys. Lett. A **54**, 425 (1975).
23. S.A. Werner, R. Colella, A.W. Overhauser, and C.F. Eagen, Phys. Rev. Lett. **35**, 1053 (1975).
24. E.P. Wigner, Am. J. Phys. **31**, 6 (1963).
25. J. Summhammer, G. Badurek, H. Rauch, U. Kischko, and A. Zeilinger, Phys. Rev. A **27**, 2523 (1983).
26. G.M. Drabkin and R.A. Zhitnikov, Sov. Phys. JETP **11**, 729 (1960).
27. B. Alefeld, G. Badurek, and H. Rauch, Z. Phys. B **41**, 231 (1981).
28. G. Badurek, H. Rauch, and J. Summhammer, Phys. Rev. Lett. **51**, 1015 (1983).
29. J. Summhammer, K.A. Hamacher, H. Kaiser, H. Weinfurter, D.L. Jacobson, and S.A. Werner, Phys. Rev. Lett. **75**, 3206 (1995).
30. G. Badurek, H. Rauch, and D. Tuppinger, Phys. Rev. A **34**, 2600 (1986).
31. B.D. Josephson, Rev. Mod. Phys. **46**, 251 (1974).
32. J. Summhammer, H. Rauch, and D. Tuppinger, Phys. Rev. A **36**, 4447 (1987).
33. H. Rauch, J. Summhammer, M. Zawisky, and E. Jericha, Phys. Rev. A **42**, 3726 (1990).
34. M. Namiki and S. Pascazio, Phys. Lett. A **147**, 430 (1990).
35. J. Bell, Physics **1**, 195 (1965).
36. H. Rauch and J. Summhammer, Phys. Rev. **46**, 7284 (1992).
37. W.K. Wooters and W.H. Zurek, Phys. Rev. D **19**, 473 (1979).
38. G. Jaeger, A. Shimony, and L. Vaidman, Phys. Rev. A **51**, 54 (1995).
39. B.-G. Englert, Phys. Rev. Lett. **77**, 2154 (1996).
40. H. Rauch, Phys. Lett. A **173**, 240 (1993).
41. D.L. Jacobson, S.A. Werner, and H. Rauch, Phys. Rev. A **49**, 3196 (1994).
42. M. Zawisky, H. Rauch, and Y. Hasegawa, Phys. Rev. A **50**, 5000 (1994).
43. M. Heinrich, D. Petrascheck, and H. Rauch, Z. Physik B **72**, 357 (1988).
44. W. Schleich and J.A. Wheeler, Nature **326**, 574 (1987).
45. A. Legett, in Proc. Int. Symp. on Found. Quantum Mechanics, edited by S. Kamefuchi (Phys. Soc. Japan, Tokyo, 1984), p. 74.
46. W. Schleich and M. Pernigo, and Fam Le Kien, Phys. Rev. A **44**, 2172 (1991).
47. D.F. Walls and G.J. Milburn, Phys. Rev. A **31**, 2403 (1985).
48. H. Zurek, Physics Today, Oct. 1991, p. 36.
49. P. Blanchard and A. Jadczyk, Phys. Lett. A **175**, 157 (1993).
50. V. Buzek, C.H. Keitel, and P.L. Knight, Phys. Rev. A **51**, 2594 (1995).
51. D.F. Walls, Nature **306**, 141 (1983).
52. R. Loudon and P.L. Knight, J. Mod. Opt. **34**, 709 (1987).
53. J. Jansky and A.V. Vinogradov, Phys. Rev. Lett. **64**, 2771 (1990).
54. E. Wolf, Phys. Rev. Lett. **63**, 2220 (1989).
55. R. Clothier, H. Kaiser, S.A. Werner, H. Rauch, and H. Wölwitsch, Phys. Rev. A **44**, 5357 (1991).
56. H. Rauch, J. Phys.: Conf. Series **36**, 164 (2006).
57. H. Rauch, Phys. Scr. T **135**, 014027 (2009)
58. S. Pancharatram, Proc. Indian Acad. Sci. A **44**, 247 (1956).
59. M.V. Berry, Proc. Royal Soc. London A **392**, 45 (1984).
60. Y. Aharonov and J. Anandan, Phys. Rev. Lett. **58**, 1593 (1987).
61. A.G. Wagh, V.C. Rakhecha, J. Summhammer, G. Badurek, H. Weinfurter, B.M. Allman, H. Kaiser, K. Hamacher, D.L. Jacobson, and S.A. Werner, Phys. Rev. Lett. **78**, 755 (1997).
62. B.E. Allman, A. Cimmino, A.G. Klein, G.I. Opat, H. Kaiser, and S.A. Werner, Phys. Rev. Lett. **68**, 2409 (1992).
63. A. Cimmino, G.I. Opat, A.G. Klein, H. Kaiser, S.A. Werner, M. Arif, and R. Clothier, Phys. Rev. Lett. **68**, 380 (1989).
64. S. Filipp, J. Klepp, Y. Hasegawa, C. Plonka-Spehr, U. Schmidt, P. Geltenbort, and H. Rauch, Phys. Rev. Lett. **102**, 030404 (2009)
65. J. Samuel and R. Bhandari, Phys. Rev. Lett. **60**, 2339 (1988).

66. S. Basu, S. Bandyopadhyay, G. Kar, and D. Home, Phys. Lett. A **270**, 281 (2001).
67. Y. Hasegawa, R. Loidl, G. Badurek, M. Baron, and H. Rauch, Nature **425**, 46 (2002).
68. S. Filipp, Y. Hasegawa, R. Loidl, and H. Rauch, Phys. Rev. A **72**, 021602 (2005).
69. G. DeChiara and G.M. Palma, Phys. Rev. Lett. **91**, 090404 (2003).
70. A. Einstein, B. Podolsky, and N. Rosen, Phys. Rev. **47**, 777 (1935).
71. D.M. Greenberger, M.A. Horne, and A. Zeilinger, in Bell's Theorem, Quantum Theory and Conceptions of the Universe, edited by M. Kafatos (Kluwer, Dordrecht, 1989), p. 69.
72. S.J. Bell, *Speakable and Unspeakable in Quantum Mechanics* (Cambridge Univ. Press, Cambridge, 1987).
73. A. Aspect, P. Grangier, and G. Roger, Phys. Rev. Lett. **49**, 91 (1982).
74. Z.Y. Ou and L. Mandel, Phys. Rev. Lett. **61**, 50 (1988).
75. G. Weihs, T. Jennewein, C. Simon, H. Weinfurter, and A. Zeilinger, Phys. Rev. Lett. **81**, 5039 (1998).
76. X.Y. Zou, T.P. Grayson, and L. Mandel, Phys. Rev. Lett. **69**, 3041 (1992).
77. H. Bartosik, J. Klepp, C. Schmitzer, S. Sponar, A. Cabello, H. Rauch, and Y. Hasegawa, Phys. Rev. Lett. **103**, 040403 (2009).
78. S. Kochen and F.P. Specker, J. Math. Mech. **17**, 59 (1967).
79. D. Mermin, Phys. Rev. Lett. **65**, 1838 (1990).
80. Y. Hasegawa, R. Loidl, G. Badurek, M. Baron, and H. Rauch, Phys. Rev. Lett. **97**, 230401 (2006).
81. C. Simon, M. Zukovski, H. Weinfurter, and A. Zeilinger, Phys. Rev. Lett. **85**, 1783 (2000).
82. C. Cinelli, M. Barbieri, P. Mataloni, and F. De Martini, Phys. Rev. Lett. **95**, 240405 (2005).
83. A. Cabello, S. Filipp, H. Rauch, and Y. Hasegawa, Phys. Rev. Lett. **100**, 130404 (2008).
84. S. Sponar, J. Klepp, R. Loidl, S. Filipp, G. Badurek, and H. Rauch, Phys. Rev. A **78**, 061604 (2008).
85. T.M. Nieuwenhuizen, Found. Phys. **41**, 580 (2011).
86. H.A. Lorentz, *Theorie der Strahlung* (Akademische Verlagsgesellschaft, Leipzig, 1927).
87. I. Prigogine, in *Proc. Ecol. Phys. Chem., Siena* (Elsevier, Amsterdam, 1991), p. 8.
88. F. Haag, Comm. Math. Phys. **123**, 245 (1990).
89. N. Komo, K. Machida, M. Namiki, and S. Pascazio, Phys. Rev. A **54**, 1064 (1996).

Received 15.07.11

ТАЄМНИЧІ КВАНТОВІ ЕФЕКТИ,
ЩО СПОСТЕРІГАЮТЬСЯ ЗА ДОПОМОГОЮ НЕЙТРОНІВ

Х. Раух

Р е з ю м е

За допомогою нейтронів можна спостерігати явища інтерференції за участю однієї частинки, і "переплутування ступеней вільності", тобто контекстуальність, може бути перевірено і використано експериментально. Переплутування двох фотонів чи атомів являє ситуацію, додаткову до дифракції одного фотона, нейтрона чи атома на двох щілинах. У цьому сенсі нейтрони є хорошим інструментом для перевірки квантової механіки, оскільки вони мають масу, взаємодіють з електромагнітними полями завдяки своєму магнітному моменту, беруть участь у всіх основних взаємодіях, а також чутливі до топологічних ефектів. Можна спостерігати 4π-симетрію спінорних хвильових функцій, суперпозицію спінів і інші топологічні ефекти як цікаві внутрішні особливості квантової фізики. У роботі обговорено відповідні експерименти. Показано, що експерименти з детерміністичною чи стохастичною частковою абсорбцією можуть бути описані нерівностями типу нерівностей Белла. Нещодавні експерименти з інтерференцією нейтронів на основі методів пост-відбору дозволяють обговорити квантову нелокальність і квантовий процес вимірювання. Показано, що явища інтерференції можуть проявлятися навіть коли загальна інтерференційна картина втрачає контрастність. Це свідчить про зв'язки, які зберігаються у фазовому просторі навіть у випадку просторово розділених ситуацій типу парадокса з "котом Шредінгера". Ці стани вельми недовговічні і надзвичайно чутливі до будь-яких флуктуацій і процесів, які приводять до декогерентності. Більш тонкі квантові експерименти показують також, що повне відновлення квантових етапів поза об'ємом з взаємодією стає у принципі неможливим.